FVCA8 benchmark for the Stokes and Navier-Stokes equations with the TrioCFD code – benchmark session

P.-E. Angeli, M.-A. Puscas, G. Fauchet, A. Cartalade

FVCA8 benchmark for the Stokes and Navier-Stokes equations with the TrioCFD code – benchmark session

P.-E. Angeli, M.-A. Puscas, G. Fauchet and A. Cartalade

Abstract This paper is devoted to the study of convergence orders of several numerical methods that are implemented in the TrioCFD code dedicated to the simulation of turbulent flows and heat transfer in nuclear engineering applications. The spatial discretization is based on Finite Difference-Volume or Finite Element-Volume methods. A projection method is applied to update the velocity and the pressure. The time scheme can be either explicit or implicit, and hexahedral or tetrahedral meshes can be used for simulations. In this paper, the test cases are relative to steady Stokes problems, steady and unsteady Navier-Stokes problems, and finally the well-known lid-driven cavity flow case. The latter proposes several comparisons between our simulations and numerical data already published in the literature, while the other cases yield the values of convergence orders by using the analytical solutions. The accuracy of the results obtained with TrioCFD differs according to the types of mesh used for simulations, the viscosity values or the source terms in the equations.

P.-E. Angeli
CEA–Saclay, Den – DM2S, STMF, LMSF, CEA, Université de Paris-Saclay.
Bât 451, F-91191, Gif-sur-Yvette.
e-mail: pierre-emmanuel.angeli@cea.fr

M.-A. Puscas
CEA–Saclay, Den – DM2S, STMF, LMSF, CEA, Université de Paris-Saclay.
Bât 451, F-91191, Gif-sur-Yvette, France.
e-mail: maria-adela.puscas@cea.fr

G. Fauchet
CEA–Saclay, Den – DM2S, STMF, LGLS, CEA, Université de Paris-Saclay.
Bât 451, F-91191, Gif-sur-Yvette, France.
e-mail: gauthier.fauchet@cea.fr

A. Cartalade
CEA–Saclay, Den – DM2S, STMF, LMSF, CEA, Université de Paris-Saclay.
Bât 451, F-91191, Gif-sur-Yvette, France.
e-mail: alain.cartalade@cea.fr

Key words: FVCA8 benchmarks, Stokes and Navier-Stokes equations, TrioCFD, Finite Element-Volume and Finite Difference-Volume methods.

MSC (2010)**:** 65N08, 65N12, 65N30, 76D06

1 Introduction

TrioCFD [13] is a Computational Fluid Dynamics code developed at CEA, dedicated to simulate incompressible or quasi-compressible flows in nuclear engineering applications. The code is open source [13] and massively parallel. The aim of this paper is to study the convergence order of TrioCFD numerical schemes through various 2D and 3D solutions of the Stokes and Navier-Stokes equations. The comparisons focus on a general incompressible Navier-Stokes model for newtonian flows, which writes:

$$\nabla \cdot \mathbf{u} = 0, \qquad (t, \mathbf{x}) \in (0, T] \times \mathscr{D}, \tag{1a}$$

$$\theta \mathbf{u}_t - \nu \Delta \mathbf{u} + \chi (\mathbf{u} \cdot \nabla) \mathbf{u} + \nabla p = \mathbf{f}, \qquad (t, \mathbf{x}) \in (0, T] \times \mathscr{D}, \tag{1b}$$

$$\int_{\mathscr{D}} p(\mathbf{x}, t) d\mathbf{x} = 0, \qquad t \in (0, T], \tag{1c}$$

$$(\text{if } \theta = 1)\ \mathbf{u}(\mathbf{x}, 0) = \mathbf{u}_0(\mathbf{x}) \qquad \mathbf{x} \in \mathscr{D}. \tag{1d}$$

Eq. (1a) represents the mass balance for incompressible flow where $\mathbf{u} \equiv \mathbf{u}(\mathbf{x}, t)$ is the velocity. Eq. (1b) refers to the conservation equation for momentum where ν is the kinematic viscosity, $p \equiv p(\mathbf{x}, t)$ is the pressure and $\mathbf{f}$ is a force term. The two coefficients $\theta = 0, 1$ and $\chi = 0, 1$ are introduced in order to simplify the flow model. If $\chi = 0$ the set of equations becomes the Stokes model, whereas $\chi = 1$ indicates that the Navier-Stokes model is considered. The case $\theta = 0$ (respectively $\theta = 1$) means that only the stationary (resp. unsteady) solution of the Navier-Stokes equations is considered.

The test cases of the FVCA8 benchmark are presented in Ref. [3]. The paper is organized as follows. Section 2 briefly describes the numerical schemes applied in this work. Section 3 presents comparisons with exact solutions of steady Stokes model. Section 4 presents comparisons for steady Navier-Stokes model. Section 5 presents comparisons for unsteady Navier-Stokes model. Section 6 focuses on robustness with respect to invariance property for the steady Stokes and Navier-Stokes models. Section 7 provides comparisons with literature results for the lid-driven cavity flow problem. Finally, some concluding remarks are given in Section 8.

2 Numerical schemes in TrioCFD

This section briefly describes the TrioCFD numerical schemes. The spatial discretization methods are presented in section 2.1. The projection method and time discretization scheme are presented in section 2.2.

2.1 Spatial discretizations

Two types of spatial discretization are avalaible according to the considered element type: the "Finite Difference-Volume" (FDV) method for hexahedral grids and "Finite Element-Volume" (FEV) method for tetrahedral ones. In the FDV (respectively FEV) method, the equations are discretized and solved on control volumes whereas the fluxes and the differential operators are computed by means of finite difference (respectively by finite element) approximations. The main advantage of those types of methods lies on the local conservative property.

Hereinafter are given some details about the FEV method, even if the FDV [6] is also applied for simulations. The description below is a summary of Refs. [6, 7, 9]. The FEV method can be viewed as a modification of the Crouzeix-Raviart element [5]. The discrete pressure is defined on the primary grid while the discrete velocity is defined on a face-based staggered dual grid. As in Finite Volume approches, the local equations are integrated over the control volumes. The control volumes for mass are the primal mesh cells whereas the dual mesh cells (denoted by ω hereafter) are the control volumes of impusion. The controle volume ω associated to each face is obtained by joining the gravity centers of the two adjacent cells sharing the face (see Fig. 1(b)). The fluxes and the differential operators are computed by means of a Finite Elements (FE) formulation.

Unlike the Crouzeix-Raviart element for which the pressure is piecewise constant per element, it is possible to add more freedom degrees for the pressure. Typically, the results presented in this work have been obtained by computing the pressure at the element barycenters and the element nodes. A two-dimensional example is presented on Fig. 1(a). As demonstrated in Refs. [9], the introduction of piecewise linear pressure function greatly improves the Crouzeix-Raviart element stability properties.

When discretizing the Stokes equations, Ref. [9] shows that the FEV discrete system is equivalent to the FE one, except for the right-hand side (source term). The reference also presents some proofs for inf-sup stability property, consistency and convergence with a second-order accuracy for velocity and first-order for pressure. Some superconvergence results are showed in some particular cases (when $\mathbf{f}$ can be expressed as the gradient of a regular enough function Φ), the accuracy is of third-order for velocity and second-order for pressure.

In TrioCFD, several methods have been developped for approximating the nonlinear convective term, among which upwind, MUSCL, QUICK schemes. All these methods consist in introducing upwinding to stabilize. In the present work, we use

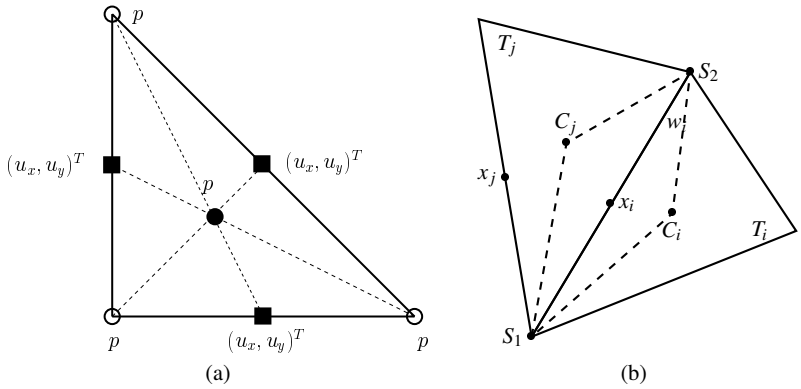

Fig. 1 (a) DoF for Crouzeix-Raviart element (black squares for velocity **u** and black dots for pressure p). In our simulations, the pressure p is also computed at vertices of each cell (circles). (b) Control volume w_i between two triangles T_i and T_j of respective center C_i and C_j. The control volume is defined by nodes C_i, S_1, C_j and S_2.

basically the upwind scheme within the FDV discretization and the MUSCL scheme within the FEV discretization. Our experience having shown that these options satisfied many cases.

2.2 Time scheme

In TrioCFD, the time discretization schemes can be either explicit (such as Forward Euler, Runge-Kutta, Adams-Bashforth, Crank-Nicholson) or implicit (such as Backward Euler and Adams-Moulton). For the steady cases the solution is obtained as the asymptotic limit of the transient state. In this case, a multiplicative factor can be applied on the time step to speed up the convergence towards the steady state. Generally, few time steps are sufficient to reach the steady state.

In order to separate the velocity and the pressure, a multi-step (projection-correction) technique [4, 12] is employed, where an intermediate velocity is computed and the mass conservation is then enforced by solving a Poisson equation for pressure. Several alternative formulations for decoupling the velocity and pressure like SIMPLE, SIMPLEC and PISO are also available in the code (see TrioCFD [13] user manual).

2.3 Benchmarks with TrioCFD

All simulations were performed with the version 1.7.3 of TrioCFD. Several options are possible for computations. They will be specified in each test case when neces-

sary. The meshes are taken from the GitHub repository [1] and converted to one format suited for TrioCFD (med format). Results of the benchmarks will be presented as mentioned in Ref. [3]. The nomenclature of tables are reminded in Appendix.

In TrioCFD, the unsteady Navier-Stokes model was applied for all simulations, even for Stokes problem by cancelling the convective term. Four types of meshes are used: squares and triangles (2D), and hexahedral and tetrahedral meshes (3D). For square and hexahedral meshes, the numerical discretization is based on the FDV method. For triangular and tetrahedral meshes the numerical discretization is based on the FEV method. The complexity tables relative to 2D grids are presented in Tabs. 2 and 4. For hexahedral meshes, the complexity table is presented in Tab. 6. For tetrahedral meshes, it is presented in Tab. 8. The time scheme is either explicit or implicit. The implicit time scheme system is solved using the iterative GMRES method and the solver used for the Poisson equation is based on a direct Cholesky factorisation.

3 Steady Stokes tests

In this section, two test cases are presented: the first one (subsection 3.1) is the "2D Bercovier–Engelman" test case [2] and the second one (subsection 3.2) is the "3D Taylor–Green vortex" [11]. For both test cases, the kinematic viscosity is set to $\nu = 1$.

3.1 The 2D Bercovier–Engelman test case

The exact solution of the 2D Bercovier–Engelman problem [2] is:

$$\mathbf{u}_{\text{ex}}(\mathbf{x}) = (u_1(x,y), -u_1(y,x))^T, \quad p_{\text{ex}}(\mathbf{x}) = \left(x - \frac{1}{2}\right)\left(y - \frac{1}{2}\right),$$

with $u_1(x,y) = -256x^2(x-1)^2y(y-1)(2y-1)$. The source term is defined by: $\mathbf{f}(\mathbf{x}) = (f_1(x,y) + (y-1/2), -f_1(y,x) + (x-1/2))^T$, with
$f_1(x,y) = 256\left[x^2(x-1)^2(12y-6) + y(y-1)(2y-1)(12x^2-12x+2)\right]$. The computational domain is $\mathscr{D} = [0,1]^2$ with non homogeneous Dirichlet boundary conditions.

The accuracy tables are presented respectively in Tabs. 1 and 3 for both mesh types. The velocity error **erru** w.r.t. the number of velocity unknowns **nnu** is presented on Fig. 2 for both type of meshes. The second-order of convergence is well-captured for cartesian meshes (red line) and triangular meshes (blue line) as confirmed by Tab. 1 and 3 respectively. On the pressure, the convergence order follows the same trend for cartesian meshes, and it is of first-order for triangular meshes.

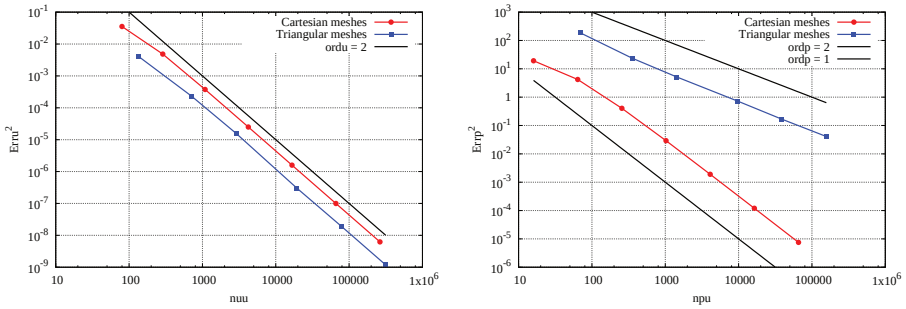

(a) (b)

Fig. 2 Convergence order on (a) velocity and (b) pressure for cartesian (red) and triangular (blue) meshes.

mesh #	**errgu**	**ordgu**	**erru**	**ordu**	**errp**	**ordp**	**errdivu**	**orddivu**
1	$6.423 \cdot 10^{-2}$	–	$6.341 \cdot 10^{-2}$	–	13.700	–	$3.278 \cdot 10^{-16}$	–
2	$4.437 \cdot 10^{-2}$	0.448	$1.528 \cdot 10^{-2}$	1.724	4.855	1.267	$2.521 \cdot 10^{-16}$	–
3	$1.797 \cdot 10^{-2}$	1.288	$3.968 \cdot 10^{-3}$	1.922	2.267	1.087	$2.695 \cdot 10^{-16}$	–
4	$4.742 \cdot 10^{-3}$	1.394	$5.474 \cdot 10^{-4}$	2.072	0.851	1.024	$3.169 \cdot 10^{-18}$	–
5	$2.044 \cdot 10^{-3}$	1.211	$1.394 \cdot 10^{-4}$	1.971	0.408	1.059	$1.98 \cdot 10^{-18}$	–
6	$9.357 \cdot 10^{-4}$	1.122	$3.444 \cdot 10^{-5}$	2.007	0.202	1.009	$8.449 \cdot 10^{-19}$	–

Table 1 Accuracy table : 2D Bercovier–Engelman - Triangle meshes

mesh #	**nuu**	**npu**	**nnzu**	**nnzp**	**nnzup**
1	136	69	1232	501	–
2	708	355	6792	2971	–
3	2878	1440	28172	12496	–
4	19462	9732	193052	86404	–
5	78012	39007	776952	348679	–
6	314056	157029	3134192	1408477	–

Table 2 Complexity table : 2D Bercovier–Engelman - Triangle meshes

mesh #	**errgu**	**ordgu**	**erru**	**ordu**	**errp**	**ordp**	**errdivu**	**orddivu**
1	$9.705 \cdot 10^{-2}$	–	0.188	–	4.380	–	$1.077 \cdot 10^{-16}$	–
2	$4.282 \cdot 10^{-2}$	1.278	$6.958 \cdot 10^{-2}$	1.554	2.050	1.095	$9.742 \cdot 10^{-17}$	–
3	$1.345 \cdot 10^{-2}$	1.741	$1.939 \cdot 10^{-2}$	1.920	0.635	1.687	$7.919 \cdot 10^{-17}$	–
4	$3.626 \cdot 10^{-3}$	1.933	$4.996 \cdot 10^{-3}$	2.001	0.171	1.896	$7.138 \cdot 10^{-17}$	–
5	$9.265 \cdot 10^{-4}$	1.991	$1.259 \cdot 10^{-3}$	2.010	$4.356 \cdot 10^{-2}$	1.971	$1.299 \cdot 10^{-18}$	–
6	$2.328 \cdot 10^{-4}$	2.002	$3.154 \cdot 10^{-4}$	2.007	$1.095 \cdot 10^{-2}$	1.991	$7.823 \cdot 10^{-19}$	–
7	$5.831 \cdot 10^{-5}$	2.002	$7.888 \cdot 10^{-5}$	2.005	$2.74 \cdot 10^{-3}$	1.998	$3.501 \cdot 10^{-19}$	–

Table 3 Accuracy table : 2D Bercovier–Engelman - Rectangle meshes

mesh #	**nuu**	**npu**	**nnzu**	**nnzp**	**nnzup**
1	80	16	164	64	–
2	288	64	652	288	–
3	1088	256	2588	1216	–
4	4224	1024	10300	4992	–
5	16640	4096	41084	20224	–
6	66048	16384	164092	81408	–
7	263168	65536	655868	326656	–

Table 4 Complexity table : 2D Bercovier–Engelman - Rectangle meshes

3.2 3D Taylor Green Vortex

The exact solution of the 3D Taylor Green Vortex [11] is:

$$\mathbf{u}_{\text{ex}} = \begin{pmatrix} -2\cos(2\pi x)\sin(2\pi y)\sin(2\pi z) \\ \sin(2\pi x)\cos(2\pi y)\sin(2\pi z) \\ \sin(2\pi x)\sin(2\pi y)\cos(2\pi z) \end{pmatrix}, \; p_{\text{ex}} = -6\pi\sin(2\pi x)\sin(2\pi y)\sin(2\pi z),$$

and the force term is defined by: $\mathbf{f} = (-36\pi^2\cos(2\pi x)\sin(2\pi y)\sin(2\pi z), 0, 0)^T$. The computational domain is $\mathscr{D} = [0,1]^3$ with non homogeneous Dirichlet boundary conditions.

The velocity error **erru** is presented on Fig. 3 (a) for both meshes. On that figure, one can see that the second-order of convergence is well-captured for hexahedral meshes (red line) as confirmed by Tab. 5. The results are less accurate for tetrahedral meshes (see Tab. 7), but the convergence order **ordu** remains superior to 1.7 for the three most refined grids (blue curve). For pressure (see Fig. 3 (b)), the second-order of convergence is well-captured for hexahedral meshes, and the accuracy is of first-order for tetrahedral meshes.

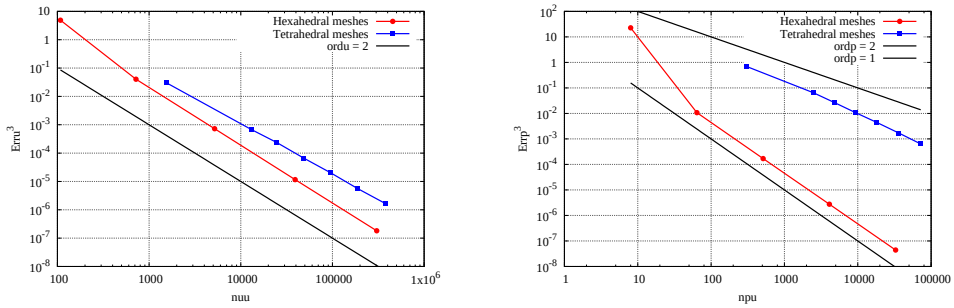

(a) (b)

Fig. 3 Convergence order on (a) velocity and (b) pressure for hexaedral (red) and tetrahedral meshes (blue).

mesh #	**errgu**	**ordgu**	**erru**	**ordu**	**errp**	**ordp**	**errdivu**	**orddivu**
1	0.421	–	1.697	–	2.828	–	0.000	–
2	1.249	−1.720	0.343	2.527	0.221	3.679	$4.844 \cdot 10^{-17}$	–
3	0.548	1.249	$8.983 \cdot 10^{-2}$	2.034	$5.533 \cdot 10^{-2}$	1.994	$2.266 \cdot 10^{-17}$	–
4	0.192	1.557	$2.264 \cdot 10^{-2}$	2.045	$1.402 \cdot 10^{-2}$	1.981	$4.911 \cdot 10^{-18}$	–
5	$7.639 \cdot 10^{-2}$	1.347	$5.664 \cdot 10^{-3}$	2.026	$3.531 \cdot 10^{-3}$	1.988	$2.146 \cdot 10^{-18}$	–

Table 5 Accuracy table : 3D Taylor–Green - Hexahedral meshes

mesh #	**nuu**	**npu**	**nnzu**	**nnzp**	**nnzup**
1	108	8	156	32	–
2	720	64	1344	352	–
3	5184	512	10848	3200	–
4	39168	4096	86592	27136	–
5	304128	32768	690816	223232	–

Table 6 Complexity table : 3D Taylor–Green - Hexahedral meshes

mesh #	**errgu**	**ordgu**	**erru**	**ordu**	**errp**	**ordp**	**errdivu**	**orddivu**
0	0.811	–	0.313	–	0.887	–	$9.931 \cdot 10^{-18}$	–
1	0.563	0.513	$8.815 \cdot 10^{-2}$	1.779	0.400	1.133	$2.141 \cdot 10^{-18}$	–
2	0.448	1.061	$6.171 \cdot 10^{-2}$	1.655	0.300	1.334	$2.151 \cdot 10^{-18}$	–
3	0.362	0.940	$4.063 \cdot 10^{-2}$	1.863	0.220	1.379	$1.78 \cdot 10^{-18}$	–
4	0.278	1.176	$2.732 \cdot 10^{-2}$	1.765	0.164	1.323	$1.213 \cdot 10^{-18}$	–
5	0.217	1.083	$1.777 \cdot 10^{-2}$	1.890	0.119	1.387	$1.799 \cdot 10^{-18}$	–
6	0.176	0.911	$1.19 \cdot 10^{-2}$	1.744	$8.608 \cdot 10^{-2}$	1.423	$9.228 \cdot 10^{-19}$	–

Table 7 Accuracy table : 3D Taylor–Green - Tetrahedral meshes

mesh #	**nuu**	**npu**	**nnzu**	**nnzp**	**nnzup**
0	1536	303	28476	3509	–
1	12960	2499	255852	31485	–
2	24744	4755	495216	60911	–
3	48498	9324	979254	120436	–
4	95127	18275	1935081	237899	–
5	188361	36172	3856923	473998	–
6	374982	72050	7718886	948404	–

Table 8 Complexity table : 3D Taylor–Green - Tetrahedral meshes

4 Steady Navier-Stokes tests and robustness with respect to viscosity coefficient value

Two steady test cases are presented here. The first one is a two-dimensional test (subsection 4.1) and the second one is a three-dimensional test (subsection 4.2). For both test cases, simulations were performed for three values of the viscosity: $\nu = 10^{-1}$, $\nu = 10^{-2}$ and $\nu = 10^{-3}$, for triangular and rectangular meshes (2D), and hexahedral and tetrahedral meshes (3D). In this paper, we present only the results for $\nu = 10^{-1}$ and $\nu = 10^{-3}$. For $\nu = 10^{-2}$, the four tables of results are given in the

folder "data" but are not presented here because the precision stands between the one obtained for $\nu = 10^{-1}$ and $\nu = 10^{-3}$.

4.1 Steady 2D tests

The simulations are carried out with two types of meshes: a triangular one and a cartesian one. The computational domain is $\mathscr{D} = [0,1]^2$ with non homogeneous Dirichlet boundary conditions. The source term is $\mathbf{f} = \mathbf{0}$. The exact solution of that problem is: $\mathbf{u}_{\text{ex}}(\mathbf{x}) = (y, -x)^T$ and $p_{\text{ex}}(\mathbf{x}) = 0.5(x^2 + y^2) - 1/3$.

In Tabs. 11 and 12, which refer to cartesian meshes for $\nu = 10^{-1}$ and $\nu = 10^{-3}$ respectively, we observe that the convergence order on velocity decreases when the viscosity decreases. Indeed, for the three most refined grids (mesh #5, #6 and #7) when $\nu = 10^{-1}$, the convergence order is **ordu** > 1.9 (see Fig. 4(a)) whereas **ordu** < 1.4 when $\nu = 10^{-3}$ (see Fig. 4(b)). When the viscosity decreases, the diffusive term influence decreases, and the convective term becomes more important. The convergence order of the solution is close to unity. The values of the convergence order on the pressure is comparable to the convergence order of the velocity.

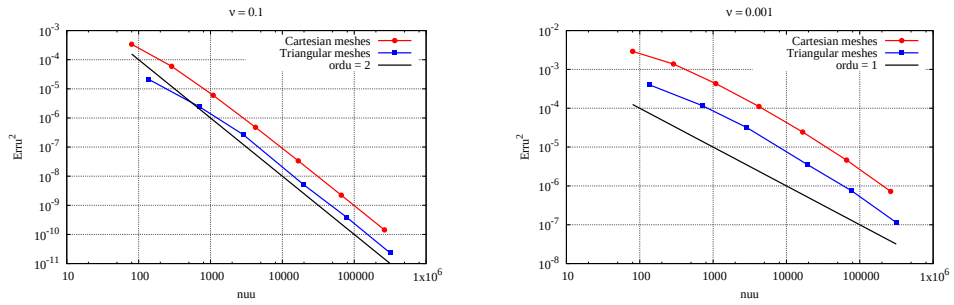

(a) (b)

Fig. 4 Convergence order on velocity for (a) $\nu = 10^{-1}$ and (b) $\nu = 10^{-3}$.

In Tabs. 9 and 10, which refer to triangular meshes, the trends are similar. The convergence orders of **u** decrease when the viscosity decreases: when $\nu = 10^{-1}$, **ordu** > 1.6 whereas **ordu** < 1.4 when $\nu = 10^{-3}$.

mesh #	**errgu**	**ordgu**	**erru**	**ordu**	**errp**	**ordp**	**errdivu**	**orddivu**
1	0.128	–	$4.646 \cdot 10^{-3}$	–	0.109	–	$1.359 \cdot 10^{-16}$	–
2	$5.756 \cdot 10^{-2}$	0.964	$1.548 \cdot 10^{-3}$	1.333	$3.597 \cdot 10^{-2}$	1.357	$1.353 \cdot 10^{-16}$	–
3	$2.647 \cdot 10^{-2}$	1.108	$5.131 \cdot 10^{-4}$	1.574	$1.057 \cdot 10^{-2}$	1.748	$1.508 \cdot 10^{-16}$	–
4	$1.078 \cdot 10^{-2}$	0.940	$7.27 \cdot 10^{-5}$	2.043	$2.163 \cdot 10^{-3}$	1.660	$3.172 \cdot 10^{-18}$	–
5	$5.074 \cdot 10^{-3}$	1.085	$1.981 \cdot 10^{-5}$	1.873	$6.996 \cdot 10^{-4}$	1.626	$1.221 \cdot 10^{-18}$	–
6	$2.515 \cdot 10^{-3}$	1.007	$4.835 \cdot 10^{-6}$	2.024	$2.219 \cdot 10^{-4}$	1.648	$6.942 \cdot 10^{-19}$	–

Table 9 Accuracy table : 2D Steady Navier-Stokes - Triangular meshes - $\nu = 10^{-1}$

mesh #	**errgu**	**ordgu**	**erru**	**ordu**	**errp**	**ordp**	**errdivu**	**orddivu**
1	0.140	–	$2 \cdot 10^{-2}$	–	0.128	–	$1.275 \cdot 10^{-16}$	–
2	$8.367 \cdot 10^{-2}$	0.627	$1.084 \cdot 10^{-2}$	0.741	$5.241 \cdot 10^{-2}$	1.092	$8.956 \cdot 10^{-17}$	–
3	$5.168 \cdot 10^{-2}$	0.687	$5.644 \cdot 10^{-3}$	0.931	$2.202 \cdot 10^{-2}$	1.238	$7.498 \cdot 10^{-17}$	–
4	$2.678 \cdot 10^{-2}$	0.687	$1.876 \cdot 10^{-3}$	1.151	$6.286 \cdot 10^{-3}$	1.312	$2.521 \cdot 10^{-18}$	–
5	$1.557 \cdot 10^{-2}$	0.782	$8.615 \cdot 10^{-4}$	1.121	$2.74 \cdot 10^{-3}$	1.195	$1.196 \cdot 10^{-18}$	–
6	$8.18 \cdot 10^{-3}$	0.924	$3.378 \cdot 10^{-4}$	1.345	$1.041 \cdot 10^{-3}$	1.389	$6.004 \cdot 10^{-19}$	–

Table 10 Accuracy table : 2D Steady Navier-Stokes - Triangular meshes - $\nu = 10^{-3}$

mesh #	**errgu**	**ordgu**	**erru**	**ordu**	**errp**	**ordp**	**errdivu**	**orddivu**
1	0.135	–	$1.843 \cdot 10^{-2}$	–	0.137	–	$4.903 \cdot 10^{-17}$	–
2	$7.089 \cdot 10^{-2}$	1.009	$7.694 \cdot 10^{-3}$	1.365	$5.859 \cdot 10^{-2}$	1.229	$4.801 \cdot 10^{-17}$	–
3	$3.539 \cdot 10^{-2}$	1.045	$2.451 \cdot 10^{-3}$	1.720	$2.116 \cdot 10^{-2}$	1.467	$3.771 \cdot 10^{-17}$	–
4	$1.727 \cdot 10^{-2}$	1.057	$6.913 \cdot 10^{-4}$	1.867	$6.765 \cdot 10^{-3}$	1.645	$3.804 \cdot 10^{-17}$	–
5	$8.417 \cdot 10^{-3}$	1.048	$1.833 \cdot 10^{-4}$	1.935	$2.004 \cdot 10^{-3}$	1.756	$8.896 \cdot 10^{-19}$	–
6	$4.13 \cdot 10^{-3}$	1.032	$4.716 \cdot 10^{-5}$	1.968	$5.643 \cdot 10^{-4}$	1.826	$4.974 \cdot 10^{-19}$	–
7	$2.04 \cdot 10^{-3}$	1.020	$1.196 \cdot 10^{-5}$	1.986	$1.546 \cdot 10^{-4}$	1.868	$2.284 \cdot 10^{-19}$	–

Table 11 Accuracy table : 2D Steady Navier-Stokes - Rectangular meshes - $\nu = 10^{-1}$

mesh #	**errgu**	**ordgu**	**erru**	**ordu**	**errp**	**ordp**	**errdivu**	**orddivu**
1	0.176	–	$5.4 \cdot 10^{-2}$	–	0.191	–	$7.23 \cdot 10^{-17}$	–
2	0.155	0.203	$3.71 \cdot 10^{-2}$	0.587	0.115	0.727	$6.669 \cdot 10^{-17}$	–
3	0.128	0.282	$2.077 \cdot 10^{-2}$	0.872	$6.265 \cdot 10^{-2}$	0.882	$5.204 \cdot 10^{-17}$	–
4	$9.522 \cdot 10^{-2}$	0.438	$1.052 \cdot 10^{-2}$	1.002	$3.15 \cdot 10^{-2}$	0.991	$3.901 \cdot 10^{-17}$	–
5	$6.314 \cdot 10^{-2}$	0.599	$4.944 \cdot 10^{-3}$	1.101	$1.479 \cdot 10^{-2}$	1.090	$9.569 \cdot 10^{-19}$	–
6	$3.745 \cdot 10^{-2}$	0.757	$2.149 \cdot 10^{-3}$	1.208	$6.415 \cdot 10^{-3}$	1.205	$5.011 \cdot 10^{-19}$	–
7	$1.977 \cdot 10^{-2}$	0.924	$8.499 \cdot 10^{-4}$	1.342	$2.519 \cdot 10^{-3}$	1.347	$2.293 \cdot 10^{-19}$	–

Table 12 Accuracy table : 2D Steady Navier-Stokes - Rectangular meshes - $\nu = 10^{-3}$

4.2 Steady 3D tests

The three-dimensional analytical solution of this problem is: $\mathbf{u}_{\text{ex}}(\mathbf{x}) = (y-z, z-x, x-y)^T$ and $p_{\text{ex}}(\mathbf{x}) = (x^2+y^2+z^2) - xy - xz - yz - 1/4$. The accuracy results are presented in Tabs. 13 and 14 for hexahedral meshes and Tabs. 15 and 16 for tetrahedral meshes. For this benchmark, the convergence order on velocity is almost of second-order when $\nu = 10^{-1}$ for hexahedral and tetrahedral meshes. The results are much less accurate when $\nu = 10^{-3}$. They are of first-order of convergence.

mesh #	**errgu**	**ordgu**	**erru**	**ordu**	**errp**	**ordp**	**errdivu**	**orddivu**
1	0.433	–	$1.914 \cdot 10^{-2}$	–	0.362	–	$1.695 \cdot 10^{-17}$	–
2	0.225	1.031	$1.611 \cdot 10^{-2}$	0.273	0.164	1.142	$1.182 \cdot 10^{-17}$	–
3	0.117	0.990	$6.63 \cdot 10^{-3}$	1.349	$7.427 \cdot 10^{-2}$	1.142	$6.809 \cdot 10^{-18}$	–
4	$5.985 \cdot 10^{-2}$	0.998	$2.188 \cdot 10^{-3}$	1.643	$2.891 \cdot 10^{-2}$	1.360	$3.079 \cdot 10^{-18}$	–
5	$3.011 \cdot 10^{-2}$	1.005	$6.329 \cdot 10^{-4}$	1.816	$9.679 \cdot 10^{-3}$	1.577	$5.806 \cdot 10^{-20}$	–

Table 13 Accuracy table : 3D Steady Navier-Stokes - Hexahedral meshes - $\nu = 10^{-1}$

mesh #	**errgu**	**ordgu**	**erru**	**ordu**	**errp**	**ordp**	**errdivu**	**orddivu**
1	0.433	–	$4.457 \cdot 10^{-2}$	–	0.377	–	$4.551 \cdot 10^{-17}$	–
2	0.244	0.907	$6.39 \cdot 10^{-2}$	−0.569	0.239	0.658	$2.19 \cdot 10^{-17}$	–
3	0.179	0.468	$5.126 \cdot 10^{-2}$	0.334	0.157	0.607	$1.66 \cdot 10^{-17}$	–
4	0.143	0.338	$3.096 \cdot 10^{-2}$	0.749	$8.952 \cdot 10^{-2}$	0.808	$5.316 \cdot 10^{-18}$	–
5	0.104	0.453	$1.581 \cdot 10^{-2}$	0.983	$4.546 \cdot 10^{-2}$	0.976	$5.597 \cdot 10^{-20}$	–

Table 14 Accuracy table : 3D Steady Navier-Stokes - Hexahedral meshes - $\nu = 10^{-3}$

mesh #	**errgu**	**ordgu**	**erru**	**ordu**	**errp**	**ordp**	**errdivu**	**orddivu**
0	0.282	–	$3.947 \cdot 10^{-2}$	–	0.549	–	$6.407 \cdot 10^{-18}$	–
1	0.161	0.791	$1.012 \cdot 10^{-2}$	1.914	0.202	1.420	$1.872 \cdot 10^{-18}$	–
2	0.136	0.778	$7.035 \cdot 10^{-3}$	1.683	0.164	0.961	$1.17 \cdot 10^{-18}$	–
3	0.122	0.476	$5.693 \cdot 10^{-3}$	0.945	0.115	1.597	$7.115 \cdot 10^{-19}$	–
4	0.100	0.878	$3.701 \cdot 10^{-3}$	1.921	$8.786 \cdot 10^{-2}$	1.194	$5.748 \cdot 10^{-19}$	–
5	$8.825 \cdot 10^{-2}$	0.561	$2.38 \cdot 10^{-3}$	1.934	$6.402 \cdot 10^{-2}$	1.387	$2.985 \cdot 10^{-19}$	–
6	$7.78 \cdot 10^{-2}$	0.549	$1.788 \cdot 10^{-3}$	1.247	$5.121 \cdot 10^{-2}$	0.970	$2.05 \cdot 10^{-19}$	–

Table 15 Accuracy table : 3D Steady Navier-Stokes - Tetrahedral meshes - $\nu = 10^{-1}$

mesh #	**errgu**	**ordgu**	**erru**	**ordu**	**errp**	**ordp**	**errdivu**	**orddivu**
0	0.327	–	0.133	–	0.239	–	$6.369 \cdot 10^{-18}$	–
1	0.183	0.814	$3.479 \cdot 10^{-2}$	1.890	0.118	1.002	$2.309 \cdot 10^{-18}$	–
2	0.169	0.384	$3.042 \cdot 10^{-2}$	0.621	0.104	0.592	$1.125 \cdot 10^{-18}$	–
3	0.152	0.472	$2.418 \cdot 10^{-2}$	1.025	$8.739 \cdot 10^{-2}$	0.774	$9.362 \cdot 10^{-19}$	–
4	0.131	0.659	$1.907 \cdot 10^{-2}$	1.056	$6.696 \cdot 10^{-2}$	1.185	$5.91 \cdot 10^{-19}$	–
5	0.120	0.394	$1.617 \cdot 10^{-2}$	0.723	$5.171 \cdot 10^{-2}$	1.137	$2.915 \cdot 10^{-19}$	–
6	0.106	0.505	$1.297 \cdot 10^{-2}$	0.963	$3.975 \cdot 10^{-2}$	1.145	$2.112 \cdot 10^{-19}$	–

Table 16 Accuracy table : 3D Steady Navier-Stokes - Tetrahedral meshes - $\nu = 10^{-3}$

5 Unsteady 2D Navier-Stokes test

In this section, the unsteady 2D Navier-Stokes equations are considered. The simulations are carried out with two types of meshes: a triangular one and a cartesian one, and for two values of the viscosity $\nu = 10^{-1}$ and $\nu = 10^{-2}$. The computational domain is $\mathscr{D} = [0,1]^2$ with non homogeneous Dirichlet boundary conditions and the final time is set to $T = \frac{1}{10\nu}$. The source term is $\mathbf{f} = \mathbf{0}$. The exact solution of the problem considered here is given by: $\mathbf{u}_{\text{ex}}(\mathbf{x}) = (\partial_y \psi, -\partial_x \psi)$, with $\psi = e^{-5\nu\pi^2 t}\cos(\pi x)\cos(2\pi y)$, and $p_{\text{ex}}(\mathbf{x}) = -\frac{1}{4}e^{-10\nu\pi^2 t}\pi^2(4\cos(2\pi x) + \cos(4\pi y))$.

The time discretization scheme employed here is the explicit third order Runge-Kutta. For this test case, when the cartesian meshes are considered, the QUICK scheme for discretizing the convective term was employed.

In Tabs. 19 and 20, which refer to cartesian meshes for $\nu = 10^{-1}$ and $\nu = 10^{-2}$ respectively, we observe that the convergence orders decrease when the viscosity decreases.The convergence order on velocity is almost of second-order when $\nu = 10^{-1}$ and first-order when $\nu = 10^{-2}$. In Tabs. 17 and 18, which refer to triangular meshes, the trends are similar.

mesh #	**errgu**	**ordgu**	**erru**	**ordu**	**errp**	**ordp**	**errdivu**	**orddivu**
1	0.101	–	0.291	–	0.493	–	$5.885 \cdot 10^{-16}$	–
2	$3.633 \cdot 10^{-2}$	1.242	$5.819 \cdot 10^{-2}$	1.950	0.150	1.456	$4.249 \cdot 10^{-16}$	–
3	$1.501 \cdot 10^{-2}$	1.259	$1.52 \cdot 10^{-2}$	1.915	$8.216 \cdot 10^{-2}$	0.857	$3.368 \cdot 10^{-16}$	–
4	$5.738 \cdot 10^{-3}$	1.006	$2.337 \cdot 10^{-3}$	1.959	$2.918 \cdot 10^{-2}$	1.083	$3.444 \cdot 10^{-16}$	–
5	–	–	$6.311 \cdot 10^{-4}$	1.886	$1.72 \cdot 10^{-2}$	0.760	$3.475 \cdot 10^{-16}$	–
6	–	–	$1.635 \cdot 10^{-4}$	1.938	$6.873 \cdot 10^{-3}$	1.318	$4.191 \cdot 10^{-16}$	–

Table 17 Accuracy table : 2D Unsteady Navier-Stokes - Triangular meshes - $\nu = 10^{-1}$

mesh #	**errgu**	**ordgu**	**erru**	**ordu**	**errp**	**ordp**	**errdivu**	**orddivu**
1	$5.033 \cdot 10^{-2}$	–	0.386	–	0.527	–	$3.307 \cdot 10^{-15}$	–
2	$2.399 \cdot 10^{-2}$	0.898	$8.914 \cdot 10^{-2}$	1.775	$9.395 \cdot 10^{-2}$	2.103	$1.789 \cdot 10^{-15}$	–
3	$9.94 \cdot 10^{-3}$	1.256	$2.358 \cdot 10^{-2}$	1.897	$3.426 \cdot 10^{-2}$	1.441	$1.457 \cdot 10^{-15}$	–
4	$3.283 \cdot 10^{-3}$	1.157	$4.636 \cdot 10^{-3}$	1.700	$1.036 \cdot 10^{-2}$	1.252	$1.316 \cdot 10^{-15}$	–
5	–	–	$1.669 \cdot 10^{-3}$	1.472	$1.057 \cdot 10^{-2}$	$-3 \cdot 10^{-2}$	$1.204 \cdot 10^{-15}$	–
6	–	–	$5.116 \cdot 10^{-4}$	1.698	$1.042 \cdot 10^{-3}$	3.326	$1.204 \cdot 10^{-15}$	–

Table 18 Accuracy table : 2D Unsteady Navier-Stokes - Triangular meshes - $\nu = 10^{-2}$

mesh #	**errgu**	**ordgu**	**erru**	**ordu**	**errp**	**ordp**	**errdivu**	**orddivu**
1	0.158	–	$7.377 \cdot 10^{-2}$	–	0.247	–	$1.552 \cdot 10^{-16}$	–
2	$6.991 \cdot 10^{-2}$	1.275	$3.596 \cdot 10^{-2}$	1.123	0.143	0.790	$1.376 \cdot 10^{-16}$	–
3	$4.099 \cdot 10^{-2}$	0.803	$1.748 \cdot 10^{-2}$	1.084	$5.144 \cdot 10^{-2}$	1.470	$1.065 \cdot 10^{-16}$	–
4	$1.879 \cdot 10^{-2}$	1.150	$6.159 \cdot 10^{-3}$	1.538	$1.8 \cdot 10^{-2}$	1.515	$9.659 \cdot 10^{-17}$	–
5	$7.747 \cdot 10^{-3}$	1.292	$2.148 \cdot 10^{-3}$	1.537	$6.3 \cdot 10^{-3}$	1.515	$8.337 \cdot 10^{-17}$	–
6	$2.977 \cdot 10^{-3}$	1.386	$6.764 \cdot 10^{-4}$	1.675	$2.044 \cdot 10^{-3}$	1.622	$8.141 \cdot 10^{-17}$	–
7	$1.094 \cdot 10^{-3}$	1.448	$1.933 \cdot 10^{-4}$	1.813	$6.217 \cdot 10^{-4}$	1.718	$7.976 \cdot 10^{-17}$	–

Table 19 Accuracy table : 2D Unsteady Navier-Stokes - Rectangular meshes - $\nu = 10^{-1}$

mesh #	**errgu**	**ordgu**	**erru**	**ordu**	**errp**	**ordp**	**errdivu**	**orddivu**
1	$5.629 \cdot 10^{-2}$	–	0.174	–	0.266	–	$1.577 \cdot 10^{-15}$	–
2	$3.493 \cdot 10^{-2}$	0.745	$7.206 \cdot 10^{-2}$	1.379	0.144	0.880	$1.265 \cdot 10^{-15}$	–
3	$4.279 \cdot 10^{-2}$	−0.305	$4.713 \cdot 10^{-2}$	0.637	$5.163 \cdot 10^{-2}$	1.480	$7.211 \cdot 10^{-16}$	–
4	$2.681 \cdot 10^{-2}$	0.690	$1.648 \cdot 10^{-2}$	1.550	$1.374 \cdot 10^{-2}$	1.910	$6.248 \cdot 10^{-16}$	–
5	$1.362 \cdot 10^{-2}$	0.986	$5.668 \cdot 10^{-3}$	1.556	$7.711 \cdot 10^{-3}$	0.834	$4.585 \cdot 10^{-16}$	–
6	$6.195 \cdot 10^{-3}$	1.142	$2.598 \cdot 10^{-3}$	1.131	$4.681 \cdot 10^{-3}$	0.719	$3.623 \cdot 10^{-16}$	–
7	$2.63 \cdot 10^{-3}$	1.240	$1.158 \cdot 10^{-3}$	1.170	$2.145 \cdot 10^{-3}$	1.125	$3.048 \cdot 10^{-16}$	–

Table 20 Accuracy table : 2D Unsteady Navier-Stokes - Rectangular meshes - $\nu = 10^{-2}$

6 Robustness with respect to the invariance property

The aim of this test is to verify that the numerical discretization preserves the following invariance property of the incompressible Stokes and Navier-Stokes equations. For boundary conditions independent of pressure, if $(\mathbf{u}, p)$ is solution of equations with the right-hand side $\mathbf{f}$, then $(\mathbf{u}, p + \psi)$ is solution of equations with the right-hand side $\mathbf{f} + \nabla\psi$.

6.1 Test on the 2D steady Stokes system

In this section, we focus on the invariance property of the 2D steady Stokes equations. For homogeneous Dirichlet conditions on velocity, if the forcing term is chosen such as $\mathbf{f} = \nabla\psi$, then we must obtain $\mathbf{u} = \mathbf{0}$ and $p = \psi$. In this test case, the function ψ is set to $\psi(x,y) = \exp(-10(1-x+2y))$.

Simulations were performed on triangular and rectangular meshes (2D) for two viscosity values: $\nu = 10^{-1}$ and $\nu = 10^{-2}$. For triangular meshes, the convergence results are presented in Tabs. 21 and 22. For nomenclature definition of tables, we refer to [3]. We observe that the convergence order is almost of third-order on velocity (**codu**) and second-order on pressure (**codp**) for both viscosity values. This confirms the super-convergence result found in Ref. [9]. Tabs. 23 and 24 refer to results obtained for rectangular meshes. In this case, for both values of viscosity, we remark a second-order accuracy on velocity and pressure.

mesh #	**devgu**	**codgu**	**devu**	**codu**	**devp**	**codp**
1	$1.171 \cdot 10^{-3}$	–	$1.45 \cdot 10^{-3}$	–	0.439	–
2	$9.399 \cdot 10^{-4}$	0.265	$1.07 \cdot 10^{-4}$	3.158	0.158	1.202
3	$6.122 \cdot 10^{-5}$	3.895	$5.841 \cdot 10^{-6}$	4.148	$2.999 \cdot 10^{-2}$	2.387
4	$5.556 \cdot 10^{-6}$	2.510	$1.857 \cdot 10^{-7}$	3.607	$5.056 \cdot 10^{-3}$	1.860
5	$6.623 \cdot 10^{-7}$	3.064	$1.555 \cdot 10^{-8}$	3.573	$1.25 \cdot 10^{-3}$	2.014
6	$8.073 \cdot 10^{-8}$	3.022	$2.539 \cdot 10^{-9}$	2.601	$2.968 \cdot 10^{-4}$	2.063

Table 21 Comparison table : 2D Steady Stokes - Triangular meshes - $\nu = 10^{-1}$

mesh #	**devgu**	**codgu**	**devu**	**codu**	**devp**	**codp**
1	$1.171 \cdot 10^{-2}$	–	$1.45 \cdot 10^{-2}$	–	0.439	–
2	$9.399 \cdot 10^{-3}$	0.266	$1.07 \cdot 10^{-3}$	3.160	0.158	1.202
3	$6.122 \cdot 10^{-4}$	3.895	$5.841 \cdot 10^{-5}$	4.148	$2.999 \cdot 10^{-2}$	2.387
4	$5.556 \cdot 10^{-5}$	2.510	$1.857 \cdot 10^{-6}$	3.606	$5.056 \cdot 10^{-3}$	1.860
5	$6.623 \cdot 10^{-6}$	3.063	$1.554 \cdot 10^{-7}$	3.573	$1.25 \cdot 10^{-3}$	2.014
6	$8.073 \cdot 10^{-7}$	3.022	$2.539 \cdot 10^{-8}$	2.603	$2.968 \cdot 10^{-4}$	2.063

Table 22 Comparison table : 2D Steady Stokes - Triangular meshes - $\nu = 10^{-2}$

mesh #	**devgu**	**codgu**	**devu**	**codu**	**devp**	**codp**
1	$4.78 \cdot 10^{-3}$	–	$1.683 \cdot 10^{-3}$	–	0.153	–
2	$5.71 \cdot 10^{-3}$	-0.278	$1.014 \cdot 10^{-3}$	0.790	0.191	-0.320
3	$2.648 \cdot 10^{-3}$	1.154	$2.373 \cdot 10^{-4}$	2.184	$8.198 \cdot 10^{-2}$	1.217
4	$8.545 \cdot 10^{-4}$	1.668	$5.138 \cdot 10^{-5}$	2.256	$2.411 \cdot 10^{-2}$	1.766
5	$2.369 \cdot 10^{-4}$	1.873	$1.227 \cdot 10^{-5}$	2.088	$6.304 \cdot 10^{-3}$	1.935
6	$6.141 \cdot 10^{-5}$	1.956	$3.034 \cdot 10^{-6}$	2.026	$1.596 \cdot 10^{-3}$	1.981
7	$1.552 \cdot 10^{-5}$	1.991	$7.564 \cdot 10^{-7}$	2.010	$4.003 \cdot 10^{-4}$	1.995

Table 23 Comparison table : 2D Steady Stokes - Rectangular meshes - $\nu = 10^{-1}$

mesh #	**devgu**	**codgu**	**devu**	**codu**	**devp**	**codp**
1	$4.78 \cdot 10^{-2}$	–	$1.683 \cdot 10^{-2}$	–	0.153	–
2	$5.71 \cdot 10^{-2}$	-0.278	$1.014 \cdot 10^{-2}$	0.790	0.191	-0.320
3	$2.648 \cdot 10^{-2}$	1.156	$2.373 \cdot 10^{-3}$	2.184	$8.198 \cdot 10^{-2}$	1.217
4	$8.545 \cdot 10^{-3}$	1.668	$5.138 \cdot 10^{-4}$	2.256	$2.411 \cdot 10^{-2}$	1.766
5	$2.369 \cdot 10^{-3}$	1.871	$1.227 \cdot 10^{-4}$	2.088	$6.304 \cdot 10^{-3}$	1.935
6	$6.141 \cdot 10^{-4}$	1.957	$3.034 \cdot 10^{-5}$	2.027	$1.596 \cdot 10^{-3}$	1.981
7	$1.552 \cdot 10^{-4}$	1.989	$7.564 \cdot 10^{-6}$	2.010	$4.003 \cdot 10^{-4}$	1.995

Table 24 Comparison table : 2D Steady Stokes - Rectangular meshes - $\nu = 10^{-2}$

6.2 Test on the 2D steady Navier-Stokes system

In this section, the Navier-Stokes equations are considered. We use the lid driven cavity test described in section 7. The computational domain is $\mathscr{D} = [0,1]^2$, the viscosity is set to $\nu = 1/400$, and simulations were performed on triangular and rectangular meshes. We compare the solution obtained without source term (see section 7) to the one obtained with the source term that is defined by $\mathbf{f} = \nabla\psi$, with $\psi = \exp(-10(1-x+2y))$. Tab. 25 refers to results obtained for triangular meshes. We observe that the convergence order is almost of fourth-order on velocity and second-order on pressure. Tab. 26 refers to results obtained for rectangular meshes. We notice a second-order accuracy on velocity and pressure. These results show that both numerical schemes preserve accurately the invariance property.

mesh #	**devgu**	**codgu**	**devu**	**codu**	**devp**	**codp**
1	$6.97 \cdot 10^{-2}$	–	$8.072 \cdot 10^{-2}$	–	0.441	–
2	$8.7 \cdot 10^{-3}$	2.522	$1.211 \cdot 10^{-2}$	2.300	0.161	1.230
3	$9.544 \cdot 10^{-4}$	3.152	$7.976 \cdot 10^{-4}$	3.878	$3.003 \cdot 10^{-2}$	2.398
4	$5.165 \cdot 10^{-5}$	3.051	$2.574 \cdot 10^{-5}$	3.592	$5.074 \cdot 10^{-3}$	1.860
5	$4.557 \cdot 10^{-6}$	3.497	$1.871 \cdot 10^{-6}$	3.778	$1.254 \cdot 10^{-3}$	2.014
6	$5.132 \cdot 10^{-7}$	3.135	$1.131 \cdot 10^{-7}$	4.027	$2.979 \cdot 10^{-4}$	2.063

Table 25 Comparison table : 2D Steady Navier-Stokes - Triangular meshes - $\nu = 1/400$

mesh #	**devgu**	**codgu**	**devu**	**codu**	**devp**	**codp**
1	0.430	–	0.425	–	0.783	–
2	0.221	1.043	0.181	1.334	0.287	1.444
3	$5.152 \cdot 10^{-2}$	2.186	$3.752 \cdot 10^{-2}$	2.363	$7.001 \cdot 10^{-2}$	2.037
4	$9.779 \cdot 10^{-3}$	2.451	$7.549 \cdot 10^{-3}$	2.365	$1.633 \cdot 10^{-2}$	2.099
5	$2.11 \cdot 10^{-3}$	2.237	$1.629 \cdot 10^{-3}$	2.236	$3.954 \cdot 10^{-3}$	2.047
6	$5.075 \cdot 10^{-4}$	2.066	$3.923 \cdot 10^{-4}$	2.065	$9.738 \cdot 10^{-4}$	2.020
7	$1.221 \cdot 10^{-4}$	2.060	$9.725 \cdot 10^{-5}$	2.018	$2.41 \cdot 10^{-4}$	2.014

Table 26 Comparison table : 2D Steady Navier-Stokes - Rectangular meshes - $\nu = 1/400$

7 2D lid driven cavity tests

Simulations are carried out with two types of meshes: a triangular one and a cartesian one. The computational domain is $\mathscr{D} = [0, 1]^2$ with no-slip conditions at the boundaries $x = 0$ and $x = 1$. For $y = 0$ and $y = 1$, the two following Dirichlet boundary conditions are respectively applied: $\mathbf{u} = (0, 0)^T$ and $\mathbf{u} = (1, 0)^T$. The source term is zero $\mathbf{f} = \mathbf{0}$. For this test case, when the cartesian meshes are considered, the QUICK scheme for discretizing the convective term was employed. Simulations are carried out for four viscosity values: $\nu = 1/100$, $\nu = 1/400$, $\nu = 1/1000$ and $\nu = 1/5000$. Only tables for maximum and minimum viscosity values are presented here. All other results are given in the folder "data". The results are compared with the available results in the literature.

In Fig. 5, we present a comparison between experimental data from Ref. [8] (blue squares), Ref. [10] (green dots) and TrioCFD (solid lines) for the x- (Fig. 5(a)) and y-components (Fig. 5(b)) of the velocity. The finest triangular and rectangular meshes are considered here and the comparison is done for the maximum and minimum viscosity values. The simulations achieve a very good agreement with literature results for both mesh types and for both viscosity values.

In Tabs. 27 and 28, which refer to the finest triangular mesh for $\nu = 1/100$ and $\nu = 1/5000$ respectively, the maximum and minimum values of the stream function (along with the coordinates where they are reached) are summarized. Tabs. 23 and 24 refer to the results obtained for the finest rectangular mesh.

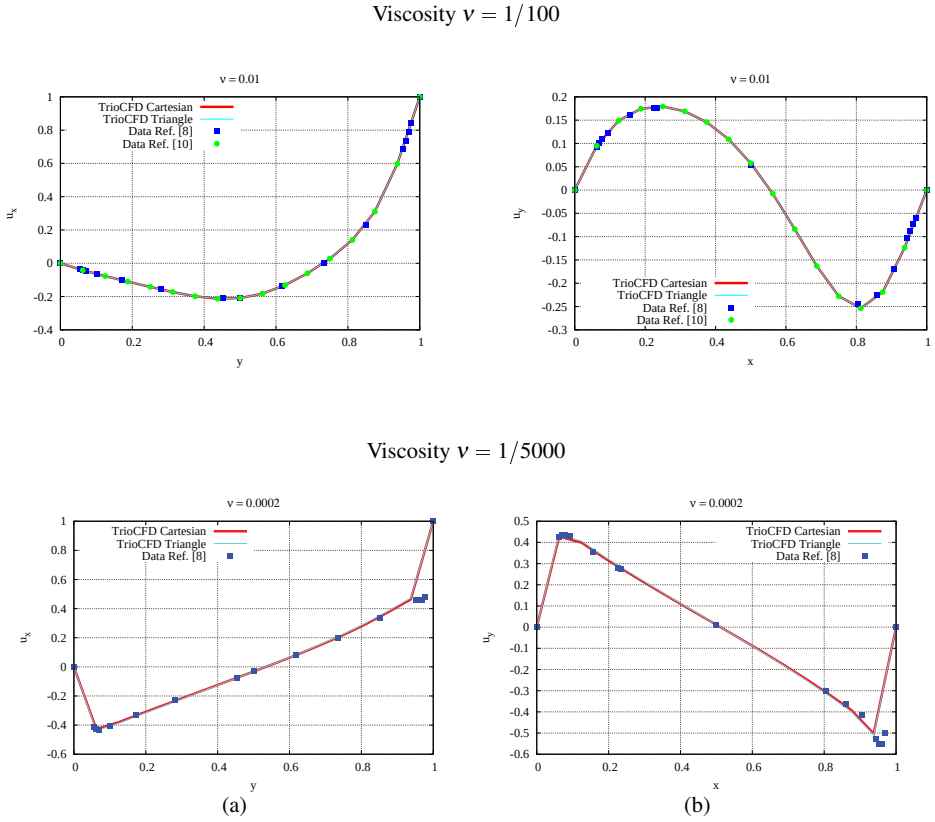

Fig. 5 Comparisons between Ref. [8] (blue squares) and Ref. [10] (green dots) with TrioCFD (solid lines). (a) u_x-component and (b) u_y-component for two viscosity values.

mesh #	$x_{\min}$	$y_{\min}$	$\psi_{\min}$	$x_{\max}$	$y_{\max}$	$\psi_{\max}$
1	0.500	0.809	-0.143	0.858	0.142	$7.904 \cdot 10^{-4}$
2	0.598	0.731	-0.103	0.908	$9.157 \cdot 10^{-2}$	$5.274 \cdot 10^{-5}$
3	0.611	0.759	-0.103	0.946	$5.396 \cdot 10^{-2}$	$1.3 \cdot 10^{-5}$
4	0.614	0.731	-0.104	0.941	$5.903 \cdot 10^{-2}$	$1.306 \cdot 10^{-5}$
5	0.614	0.741	-0.104	0.941	$5.815 \cdot 10^{-2}$	$1.27 \cdot 10^{-5}$
6	0.616	0.737	-0.104	0.944	$6.477 \cdot 10^{-2}$	$1.272 \cdot 10^{-5}$

Table 27 Stream function table : Lid driven cavity - Triangular meshes - $\nu = 1/100$

mesh #	$x_{\min}$	$y_{\min}$	$\psi_{\min}$	$x_{\max}$	$y_{\max}$	$\psi_{\max}$
1	0.500	0.809	-0.140	0.000	0.000	0.000
2	0.826	0.928	$-5.118 \cdot 10^{-2}$	0.422	0.363	$1.2 \cdot 10^{-2}$
3	0.493	0.610	-0.119	0.124	0.201	$5.27 \cdot 10^{-3}$
4	0.514	0.529	-0.125	0.795	$8.379 \cdot 10^{-2}$	$3.12 \cdot 10^{-3}$
5	0.515	0.540	-0.124	0.803	$7.008 \cdot 10^{-2}$	$3.103 \cdot 10^{-3}$
6	0.513	0.534	-0.123	0.802	$7.056 \cdot 10^{-2}$	$3.095 \cdot 10^{-3}$

Table 28 Stream function table : Lid driven cavity - Triangular meshes - $\nu = 1/5000$

mesh #	$x_{\min}$	$y_{\min}$	$\psi_{\min}$	$x_{\max}$	$y_{\max}$	$\psi_{\max}$
1	0.500	0.750	$-4.447\cdot10^{-2}$	0.000	0.000	0.000
2	0.625	0.750	$-8.415\cdot10^{-2}$	0.000	0.000	0.000
3	0.625	0.750	$-9.846\cdot10^{-2}$	0.938	$6.25\cdot10^{-2}$	$7.964\cdot10^{-5}$
4	0.625	0.750	-0.102	0.938	$6.25\cdot10^{-2}$	$2.695\cdot10^{-5}$
5	0.609	0.734	-0.103	0.938	$6.25\cdot10^{-2}$	$1.518\cdot10^{-5}$
6	0.617	0.734	-0.103	0.945	$6.25\cdot10^{-2}$	$1.318\cdot10^{-5}$
7	0.617	0.738	-0.104	0.941	$6.25\cdot10^{-2}$	$1.282\cdot10^{-5}$

Table 29 Stream function table : Lid driven cavity - Rectangular meshes - $\nu = 1/100$

mesh #	$x_{\min}$	$y_{\min}$	$\psi_{\min}$	$x_{\max}$	$y_{\max}$	$\psi_{\max}$
1	0.500	0.500	$-1.563\cdot10^{-2}$	0.000	0.000	0.000
2	0.500	0.500	$-4.653\cdot10^{-2}$	0.000	0.000	0.000
3	0.563	0.500	$-7.14\cdot10^{-2}$	0.000	0.000	0.000
4	0.531	0.531	$-8.586\cdot10^{-2}$	$6.25\cdot10^{-2}$	0.156	$5.49\cdot10^{-4}$
5	0.516	0.547	-0.104	0.797	$7.813\cdot10^{-2}$	$2.74\cdot10^{-3}$
6	0.516	0.539	-0.116	0.797	$7.813\cdot10^{-2}$	$3.297\cdot10^{-3}$
7	0.516	0.535	-0.121	0.805	$7.422\cdot10^{-2}$	$3.106\cdot10^{-3}$

Table 30 Stream function table : Lid driven cavity - Rectangular meshes - $\nu = 1/5000$

In Tabs. 31/33 (respectively Tabs. 32/34), which refer to the finest triangular mesh for $\nu = 1/100$ (resp. $\nu = 1/5000$), the horizontal/vertical velocities are given for different positions along midlines of the cavity. For the finest rectangular grid, the four tables of results are given in the folder "data" but are not presented in this paper.

Mesh #	y	0.0000	0.0625	0.1016	0.2813	0.5000	0.7344	0.9531	0.9688	1.0000
1		0.0000	−0.0290	−0.0471	−0.1328	−0.2394	−0.0612	0.7534	0.8359	1.0000
2		0.0000	−0.0370	−0.0598	−0.1491	−0.2069	−0.0036	0.7037	0.8029	1.0000
3		0.0000	−0.0410	−0.0625	−0.1542	−0.2077	0.0010	0.6826	0.7888	1.0000
4		0.0000	−0.0419	−0.0643	−0.1575	−0.2091	0.0039	0.6902	0.7917	1.0000
5		0.0000	−0.0419	−0.0644	−0.1576	−0.2092	0.0042	0.6908	0.7919	1.0000
6		0.0000	−0.0420	−0.0644	−0.1577	−0.2091	0.0042	0.6910	0.7919	1.0000

Table 31 Hor. velocity $y \mapsto u(0.5, y)$: Lid driven cavity - Triangular meshes - $\nu = 1/100$

Mesh #	y	0.0000	0.0625	0.1016	0.2813	0.5000	0.7344	0.9531	0.9688	1.0000
1		0.0000	−0.0390	−0.0635	−0.0938	−0.0338	−0.1136	0.7203	0.8139	1.0000
2		0.0000	0.0367	0.0614	0.0337	−0.0191	−0.0895	0.4519	0.6354	1.0000
3		0.0000	0.0493	−0.0526	−0.3827	−0.1167	0.1862	0.5271	0.6854	1.0000
4		0.0000	−0.4101	−0.4337	−0.2504	−0.0360	0.2115	0.4755	0.4741	1.0000
5		0.0000	−0.4347	−0.4257	−0.2427	−0.0332	0.2099	0.4827	0.4840	1.0000
6		0.0000	−0.4384	−0.4198	−0.2383	−0.0323	0.2066	0.4810	0.4807	1.0000

Table 32 Hor. velocity $y \mapsto u(0.5, y)$: Lid driven cavity - Triangular meshes - $\nu = 1/5000$

Mesh #	x	0.0000	0.0703	0.0938	0.2266	0.5000	0.8594	0.9453	0.9609	1.0000
1		0.0000	0.0733	0.0978	0.1786	0.0192	−0.1748	−0.0680	−0.0486	0.0000
2		0.0000	0.0953	0.1271	0.1722	0.0516	−0.1983	−0.0965	−0.0690	0.0000
3		0.0000	0.1011	0.1225	0.1762	0.0563	−0.2262	−0.1072	−0.0782	0.0000
4		0.0000	0.1031	0.1262	0.1791	0.0576	−0.2334	−0.1085	−0.0774	0.0000
5		0.0000	0.1035	0.1264	0.1793	0.0576	−0.2337	−0.1084	−0.0779	0.0000
6		0.0000	0.1036	0.1264	0.1793	0.0575	−0.2337	−0.1085	−0.0780	0.0000

Table 33 Ver. velocity $x \mapsto v(x, 0.5)$: Lid driven cavity - Triangular meshes - $\nu = 1/100$

Mesh #	x	0.0000	0.0703	0.0938	0.2266	0.5000	0.8594	0.9453	0.9609	1.0000
1		0.0000	0.0567	0.0757	0.1381	0.0156	−0.1424	−0.0554	−0.0396	0.0000
2		0.0000	−0.0610	−0.0815	−0.0299	0.0036	0.0460	0.0280	0.0200	0.0000
3		0.0000	0.3356	0.3589	0.3050	0.0126	−0.4033	−0.3586	−0.2649	0.0000
4		0.0000	0.4385	0.4463	0.3026	0.0103	−0.3961	−0.5424	−0.5057	0.0000
5		0.0000	0.4474	0.4476	0.2962	0.0117	−0.3856	−0.5533	−0.5607	0.0000
6		0.0000	0.4460	0.4434	0.2918	0.0118	−0.3797	−0.5446	−0.5707	0.0000

Table 34 Ver. velocity $x \mapsto v(x, 0.5)$: Lid driven cavity - Triangular meshes - $\nu = 1/5000$

8 Conclusion

In this paper, several two- and three-dimensional test cases were carried out in order to check the accuracy and convergence orders of TrioCFD. Various types of meshes were applied for those tests (rectangle, triangle, tetrahedron, hexahedron). For steady Stokes tests, the results are of second-order for velocity and pressure for rectangular and hexahedral grids. For triangular and tetrahedral grids, they are of second-order for velocity and only of first-order for pressure, as expected for the "Crouzeix-Raviart" element applied for those tests. The trends are similar for steady Navier-Stokes tests for each type of mesh. However, the convergence order for velocity decreases when the viscosity value becomes smaller because the numerical scheme for the non-linear convective term is only of first-order. The numerical scheme is robust with respect to the invariance property: a third-order accuracy is obtained for velocity and a second-order for pressure. These results do not depend on viscosity values. Finally, for the lid-driven cavity flow, excellent fittings were obtained with literature results.

Appendix: nomenclature

In this Appendix, the nomenclature of symbols (appearing in tables) is recalled in Tab. 35. The computational errors and accuracy of the results are defined by Eqs.

(2a)–(2d). In these relationships, i is the number of mesh and $d = 2$ or 3 is the space dimension. In Eq. (2a), $\|\boldsymbol{\nabla}\mathbf{u}\|^2 = \sum_{ij}(\partial u_i/\partial x_j)^2$. In Eq. (2b), $\|\mathbf{u}\|^2 = \sum_i u_i^2$. In Eq. (2c), $p^\varepsilon = (p - \int_\mathscr{D} p dV) - p_{\mathrm{ex}}$. The quantities **nuu** and **npu** are defined in Tab. 35.

Symbol	Number of
nuu	: velocity unknowns
npu	: pressure unknowns
nnzu	: non-zero terms in the velocity-velocity matrix (only for implicit time schemes)
nnzp	: non-zero terms in the pressure-pressure matrix.
nnzup	: non-zero terms in the velocity-pressure matrix. Undefined here because no velocity- pressure matrix (use of a projection method)

Table 35 Nomenclature of freedom degrees and non-zero terms.

$$\mathbf{errgu} = \left[\frac{\int_\mathscr{D}\|\boldsymbol{\nabla}(\mathbf{u}-\mathbf{u}_{\mathrm{ex}})\|^2}{\int_\mathscr{D}\|\boldsymbol{\nabla}\mathbf{u}_{\mathrm{ex}}\|^2}\right]^{1/2} \qquad \mathbf{ordgu} = -d\frac{\ln(\mathbf{errgu}_i) - \ln(\mathbf{errgu}_{i-1})}{\ln(\mathbf{nuu}_i) - \ln(\mathbf{nuu}_{i-1})} \tag{2a}$$

$$\mathbf{erru} = \left[\frac{\int_\mathscr{D}\|\mathbf{u}-\mathbf{u}_{\mathrm{ex}}\|^2}{\int_\mathscr{D}\|\mathbf{u}_{\mathrm{ex}}\|^2}\right]^{1/2} \qquad \mathbf{ordu} = -d\frac{\ln(\mathbf{erru}_i) - \ln(\mathbf{erru}_{i-1})}{\ln(\mathbf{nuu}_i) - \ln(\mathbf{nuu}_{i-1})} \tag{2b}$$

$$\mathbf{errp} = \left[\frac{\int_\mathscr{D}|p^\varepsilon|^2}{\int_\mathscr{D}|p_{\mathrm{ex}}|^2}\right]^{1/2} \qquad \mathbf{ordp} = -d\frac{\ln(\mathbf{errp}_i) - \ln(\mathbf{errp}_{i-1})}{\ln(\mathbf{npu}_i) - \ln(\mathbf{npu}_{i-1})} \tag{2c}$$

$$\mathbf{errdivu} = \left[\int_\mathscr{D}|\boldsymbol{\nabla}\cdot\mathbf{u}|^2\right]^{1/2} \qquad \mathbf{orddivu} = -d\frac{\ln(\mathbf{errdivu}_i) - \ln(\mathbf{errdivu}_{i-1})}{\ln(\mathbf{nuu}_i) - \ln(\mathbf{nuu}_{i-1})} \tag{2d}$$

References

1. URL https://github.com/FranckBoyer/FVCA8_Benchmark/tree/master/Meshes
2. Bercovier, M., Engelman, M.: A finite element for the numerical solution of viscous incompressible flows. Journal of Computational Physics **30**(2), 181 – 201 (1979). DOI http://dx.doi.org/10.1016/0021-9991(79)90098-6
3. Boyer, F., Omnes, P.: Benchmark for the FVCA8 Conference finite volume methods for the Stokes and Navier-Stokes equations. In: Finite Volume for Complex Applications 8, pp. 1–10 (2016). Https://github.com/FranckBoyer/FVCA8 _ Benchmark
4. Chorin, A.J.: Numerical solution of the Navier-Stokes equations. Mathematics of computation **22**(104), pp. 745–762 (1968)
5. Crouzeix, M., Raviart, P.A.: Conforming and nonconforming finite element methods for solving the stationary Stokes equations i. Revue française d'automatique, informatique, recherche opérationnelle. Mathématique **7**(3), pp. 33–75 (1973)
6. Emonot, P.: Méthodes de volumes éléments finis : applications aux équations de Navier-Stokes et résultats de convergence. Ph.D. thesis, Université Claude Bernard – Lyon I (1992)
7. Fortin, T.: Une méthode d'éléments finis à décomposition L2 d'ordre élevé motivée par la simulation des écoulements diphasiques bas Mach. Ph.D. thesis, Paris 6 (2006)
8. Ghia, U., Ghia, K.N., Shin, C.: High-Re solutions for incompressible flow using the Navier-Stokes equations and a multigrid method. Journal of computational physics **48**(3), 387–411 (1982)

9. Heib, S.: Nouvelles discrétisations non structurées pour les écoulements de fluides à incompressibilité renforcée. Ph.D. thesis, Université Pierre et Marie Curie (2003)
10. Marchi, C.H., Suero, R., Araki, L.K.: The lid-driven square cavity flow: numerical solution with a 1024 x 1024 grid. Journal of the Brazilian Society of Mechanical Sciences and Engineering **31**(3), 186–198 (2009)
11. Taylor, G., Green, A.: Mechanism of the production of small eddies from large ones. Proceedings of the Royal Society of London A: Mathematical, Physical and Engineering Sciences **158**(895), 499–521 (1937). DOI 10.1098/rspa.1937.0036. URL http://rspa.royalsocietypublishing.org/content/158/895/499
12. Temam, R.: Une méthode d'approximation de la solution des équations de Navier-Stokes. Bulletin de la Société Mathématique de France **96**, pp. 115–152 (1968)
13. TrioCFD: Website. URL http://www-trio-u.cea.fr/